Functional spreading of hyperexcitability induced by human and synthetic intracellular Aβ oligomers

Eduardo J. Fernandez-Perez[1,*], Braulio Muñoz[1], Denisse A. Bascuñan[1], Christian Peters[1], Nicolas O. Riffo-Lepe[1], Maria P. Espinoza[1], Peter J. Morgan[2], Caroline Filippi[2], Romain Bourboulou[2], Urmi Sengupta[3,4], Rakez Kayed[3,4], Jérôme Epsztein[2], Luis G. Aguayo[1,*].

[1] Laboratory of Neurophysiology, Department of Physiology, Universidad de Concepción, Barrio Universitario s/n P. O. Box 160-C, Concepción, Chile. Fernandez-Pérez EJ email: edfernandez@udec.cl, Muñoz B email: brauliomunoz@udec.cl, Bascuñan Muñoz DA email: denisse.bascunan.m@gmail.com, Peters C email: cpeters@udec.cl, Espinoza MP email: marespinozam@udec.cl, Riffo Lepe NO email: nriffo@udec.cl

[2] Institute of Neurobiology of the Mediterranean Sea (INMED), BP13 - 13273 Marseille cedex 09 - France. Morgan P email: peter.morgan@inserm.fr, Filippi C email: caroline.filippi@inserm.fr, Bourboulou R email: romain.bourboulou@inserm.fr, Epsztein J email: jerome.epsztein@inserm.fr

[3] Mitchell Center for Neurodegenerative Diseases, University of Texas Medical Branch, Galveston, TX, USA. [4] Department of Neurology, Neuroscience and Cell Biology, University of Texas Medical Branch, Galveston, 77555 TX, USA. Sengupta U email: ursengup@utmb.edu, Kayed R email: rakayed@utmb.edu

*To whom correspondence should be addressed:

Eduardo J. Fernandez-Perez, PhD and Luis G. Aguayo, PhD, Department of Physiology, Universidad de Concepción, P. O. Box 160-C, Concepción, Chile. Tel.: 56-41-203380; Fax: 56-41-245975; email: edfernandez@udec.cl and laguayo@udec.cl

Keywords:

AMPA-R / functional spreading / hyperexcitability / Intracellular Aβ / nitric oxide.

Abstract

Background

Intracellular amyloid-beta oligomers (iAβo) accumulation and neuronal hyperexcitability are two crucial events at early stages of Alzheimer's disease (AD). However, to date, no mechanism linking them has been reported.

Methods

Here, the effects of human AD brain-derived (h-iAβo) and synthetic (iAβo) peptides on synaptic currents and action potential (AP) firing were investigated in hippocampal neurons *in vitro*, *ex vivo* and *in vivo*.

Results

Starting from 500 pM, iAβo rapidly increased the frequency of synaptic currents and higher concentrations potentiated the AMPA receptor-mediated current. Both effects were PKC-dependent. Parallel recordings of synaptic currents and nitric oxide (NO)-related fluorescence changes indicated that the increased frequency, related to pre-synaptic release, was dependent on a NO-mediated retrograde signaling. Moreover, increased synchronization in NO production was also observed in neurons neighboring those dialyzed with iAβo, indicating that iAβo can increase network excitability at a distance. Current-clamp recordings suggested that iAβo increased neuronal excitability via AMPA-driven synaptic activity without altering membrane intrinsic properties.

Conclusion

These results strongly indicate that iAβo causes functional spreading of hyperexcitability through a synaptic-driven mechanism and offer an important neuropathological significance to intracellular species in the initial stages of AD, which include brain hyperexcitability and seizures.

1. Background

Numerous studies have reported that amyloid beta (Aβ) plays an important role in the synaptic dysfunction observed in Alzheimer's disease (AD) patients [1,2]. Unfortunately, current therapeutic targets are focused on extracellular Aβ accumulation at a stage when the disease is well underway. However, there might be previous events in the pathology that are more important in the early pre-clinical stages, thus, other mechanisms for the pathogenesis of AD need to be considered. For example, it was recently reported that prior to the formation of extracellular Aβ deposits and intracellular tau tangles in the human brain, there is an intracellular accumulation of Aβ oligomers (iAβo) during AD, especially in vulnerable regions such as the entorhinal cortex and hippocampus [3]. Moreover, it has been suggested that amyloid plaques can result from iAβo accumulation, indicating that extracellular deposits are not the exclusive origin of senile plaques [4], thus highlighting the importance of iAβo as an early stage in the progression of the pathology. The presence of iAβo has also been associated with synaptic dysfunction in different AD mice models, which could play a key role in the cognitive deficit observed in this disease. For example, the 3xTg AD model develops intraneuronal accumulation of Aβ between 3 and 4 months of age [5], a time when cognitive deficits are first detected and a stage with little, if any, presence of extracellular Aβ [6]. Interestingly, the removal of iAβo with immunotherapy improves cognition in this model [6], and as the pathology reemerges, there is a reappearance of intraneuronal Aβ followed by the formation of extracellular amyloid plaques [7]. Thus, growing evidence supports intraneuronal accumulation of Aβ as an early event in the course of the pathology, and there are studies in at least 7 other murine AD models (including 5xFAD, APP/tau, APP751SL/PS1 KI, APPE693Δ and TBA2) [8–10] that also show the presence of intraneuronal Aβ prior to extracellular accumulation, independent of the mutation they carry.

Early intracellular Aβ accumulation is particularly interesting since recent evidence has shown that changes in neuronal excitability could also be playing a fundamental role in the initial stages of Aβ pathology, predisposing the development of a synaptopathy postulated in the initial stages of AD. For example, subjects diagnosed in the early stages of prodromal AD (a very early

form of AD) displayed increased neuronal activity in the hippocampus and cortex [11,12]. Additionally, it was found that patients might exhibit increased neuronal excitability and even present a higher risk of seizures [13–15]. Indeed, two independent studies demonstrated that seizures were present in ~10-20% of patients diagnosed with sporadic AD [16,17], and patients with familial AD with mutations in APP, PS1 and PS2 also exhibited an increased prevalence of seizures [18–20]. Moreover, these early changes in excitability in human AD brains are in agreement with *in vitro* studies that showed epileptiform activity [21] and hyper-synchronous neuronal activity following acute exposure to extracellular Aβ, as well as *in vivo* models that exhibit altered intrinsic excitability [22–24] and convulsive neuronal activity [23,25]. The nature of this hyperexcitability is currently unknown.

Since intraneuronal accumulation is an early event in the pathology, these studies suggest a potential link between iAβo and neuronal hyperexcitability. However, a potential cellular mechanism that might explain this potential association has not been reported. Here, we describe that h-iAβo and iAβo applied to the postsynaptic neuron increased global synaptic transmission, excitability, and neuronal synchronization in different *in vitro* and *in vivo* hippocampal models. The presynaptic action of iAβo was primarily caused by a NO-dependent retrograde signaling, while the postsynaptic effect was mediated by the potentiation in AMPA currents by a PKC-dependent mechanism.

2. Methods

Detailed description of the applied methods are provided in Additional file 1: Supplementary methods

2.1. Primary cultures of rat hippocampal neurons. Hippocampal neurons were obtained from 18-day embryos from pregnant Sprague-Dawley rats and cultured for 10-14 days *in vitro* (DIV) as previously described [94].

2.2. Preparation of amyloid beta oligomers. Human Aβ42 fluorescently labeled with FAM (5 (6) – Carboxyfluorescein) at the N-terminal or without fluorescence were bought from Biomatic (USA) and Genemed Synthesis Inc. (USA), respectively. Synthetic oligomeric species of Aβ (later referred as iAβo) were prepared as previously described [95]. See details in Additional file 1: Supplementary methods, section 1.1.

2.3. Obtaining human-derived Aβo. Oligomeric assemblies of Aβ were derived from AD brain tissues (later referred as h-iAβo) by following previously published protocol [96]. Aβo was extracted from the PBS-soluble fraction of AD brain homogenate using co-Immunoprecipitation Kit (ThermoFisher Scientific, USA) following manufacturer's guidelines. Briefly, amine-reactive resin was coupled with anti-Aβ 6E10 antibody (BioLegend, USA) followed by incubation with PBS-soluble fraction of AD brain homogenate. Bound proteins were eluted in 0.1 M glycine (pH 2.8), and the final pH was adjusted to 7.0 by adding 1 M Tris-HCl (pH 8). Eluted fraction was subjected to buffer exchange and collected in sterile PBS. This fraction was further separated by size exclusion chromatography using AKTA Explorer system fitted with a Superdex 200 Increase 10/300 GL Column. Degassed PBS was used as mobile phase with a flowrate of 0.5 mL/min to collect the Aβo fraction. The total protein concentration was measured with bicinchoninic acid protein assay (Pierce™ Micro BCA Kit, ThermoFisher Scientific, USA). Human brain-derived Aβo was characterized by Western blot analysis and atomic force microscopy (details in Additional file 1: Supplementary methods, section 1.2 and 1.3).

2.4. Electrophysiology. Whole cell recordings were used to simultaneously apply Aβ peptide intracellularly through the internal solution contained in the recording electrode and record post-synaptic currents at constant voltage (voltage-clamp) or action potentials (current-clamp) *in vitro, ex vivo* and/or *in vivo*.

2.4.1. Voltage-clamp experiments *in vitro* and *ex vivo*. For *in vitro* experiments, the dish culture medium was replaced with a normal external solution (NES) containing (in mM): 150 NaCl, 5.4 KCl, 2.0 CaCl2, 1.0 MgCl2, 10 glucose and 10 HEPES (pH 7.4 adjusted with NaOH, 310 mOsm / L). Cells were stabilized at room temperature for 20 minutes before beginning the experiments. Unless otherwise noted, the internal solution used to record voltage-clamp experiments, including synaptic currents or ligand-evoked currents, contained (in mM): 120 KCl, 2.0 MgCl2, 2 Na2ATP, 10 BAPTA, 0.5 NaGTP and 10 HEPES (pH 7.4 adjusted with KOH, 290 mOsm / L). To study miniature post-synaptic currents (mPSCs), 500 nM tetrodotoxin (TTX) (Alomone Labs, Israel) was applied in the NES of the well containing the cells (details in Additional file 1: Supplementary methods, section 1.5). For the AMPAergic evoked (eEPSCs) and GABAergic (eIPSCs) currents, 500 nM of TTX was used in the recording solution, and using a gravity-driven perfusion system (2-3 ml/min), 100 µM of extracellular AMPA and GABA were applied, respectively. All currents (synaptic and evoked) were recorded in voltage-clamp mode by adjusting the membrane potential to -60 mV (unless otherwise noted). Voltage-clamp *in vitro* experiments were performed using an Axopatch-200B amplifier (Molecular Devices, USA) and an inverted microscope (Nikon Eclipse TE200-U, Japan). The acquisition was made using a computer connected to the registration system using a Digidata 1440A acquisition card (Molecular Devices, USA) and the pClamp10 software (Molecular Devices, USA). Electrodes with a resistance of 4-5 MΩ were pulled from borosilicate capillaries (WPI, USA) in a horizontal puller (P1000, Sutter Instruments, USA). Some voltage-clamp experiments were performed using the following internal solution (in mM): 114 K-Gluconate, 4 KCl, 4 MgCl2, 10 BAPTA and 10 HEPES (pH 7.4 adjusted with KOH, 290 mOsm / L). This was later referred as "*low Cl^- internal solution*". Details of voltage-clamp *ex vivo* experiments in Additional file 1: Supplementary methods, section 1.5.

2.4.2. Current-clamp experiments *in vitro*. To study the membrane potential (Vm) recordings were made in current-clamp mode as previously described [97], using the previously mentioned *low Cl^- internal solution.* To evoke action potentials, a family of current pulses applied for 300 ms was used (from -300 pA to +275 pA, increasing by 25 pA steps). In some experiments, the voltage-dependent sodium channel intracellular inhibitor (QX-314) (Tocris, USA) was used. Before starting the recording of evoked action potentials, a small holding current (-2 to - 50 pA) was applied to stabilize the resting membrane potential (RMP) to -70 mV. Current-clamp *in vitro* experiments were performed using an Axopatch-200B amplifier (Molecular Devices, USA) and an inverted microscope (Nikon Eclipse TE200-U, Japan).

2.4.3. Current-clamp recordings *in vivo*. All experiments on live animals were approved by the Institut National de la Santé et de la Recherche Médicale (INSERM) Animal Care and Use Committee, in accordance with the guidelines of the European Community Council directives (2010/63/EU). Data were obtained from male Wistar rats between the ages of postnatal day 25 (P25) to P35 (weight range, 90-110 g). Recordings were made as previously described [98]. See details in in Additional file 1: Supplementary methods, section 1.6.

2.5. Histology. At the end of the recording period and to confirm the location and the morphology of *in vivo* recorded neurons, we performed immunohistochemical analysis of hippocampus sections. See details in Additional file 1: Supplementary methods, section 1.7.

2.6. Simultaneous recordings of electrophysiology and fluorescence. Simultaneous studies were performed using the same methodology described for the recording of synaptic currents in voltage-clamp mode *in vitro* (section 2.4.1) together with NO fluorescence using a previously described methodology [99]. See details in Additional file 1: Supplementary methods, section 1.8.

2.7. Data analysis. All data obtained from all parameters were plotted using OriginPro2019b (Origin Lab, USA). Data are shown as mean ± SEM for normally distributed populations and as median and interquartile ranges (IQR) for non-normally distributed populations. Statistical analyses were performed using the two-tailed unpaired Student's t-tests (α=0.05) or the two-tailed Mann-Whitney U-test (α=0.05) as appropriate, after testing for normality with Shapiro-Wilk test (for n<50) or Kolmogorov-Smirnov (for n>50) and for homogeneity of variances with Levene's test. Data with more than two groups or factors were analyzed by two-way ANOVA test (α=0.05). One-way ANOVA test was used to compare several populations of neurons, followed by Tukey or Welch's ANOVA with Games-Howell post-hoc test to correct for variance heterogeneity using R software [100] (www.r-project.com). A probability level (p) < 0.05 was considered statistically significant (* p < 0.05, ** p < 0.01, *** p < 0.001). Unless otherwise noted, all "n" values represent recorded cells (see details of parameter calculations in Additional file 1: Supplementary methods, section 1.9).

3. Results

Rapid effect of human derived iAβo in hippocampal neuronal activity

We examined the synaptic effects of human AD-brain derived intracellular oligomers (h-iAβo) using an electrophysiological approach. First, characterization of the biochemically purified Aβ species with WB analysis using A11 (anti-amyloid oligomers) and 6E10 (generic anti-Aβ) antibodies confirmed the presence of Aβo in this preparation (Fig. 1a) and AFM imaging showed a homogeneously distributed population of sphere shaped oligomers ranging from 5-20 nm in size (Fig. 1b). Using a patch electrode, we delivered increasing concentrations (0, 50 and 1000 nM) of h-iAβo while recording post-synaptic currents in primary hippocampal neurons (see scheme in Fig. 1c). Control synaptic current recordings were made with an intracellular solution without h-iAβo. Electrophysiological recordings showed the presence of spontaneous synaptic events (Fig. 1d, arrows in blue) that had a stable response over a period of 10 minutes. Applying a low concentration of h-iAβo with the patch electrode (50 nM) augmented the presence of bursts of spontaneous synaptic currents interspersed in the recording (Fig. 1d, arrowheads in middle trace). It is also possible to observe that part of the total activity is mediated by spikes in current recording mode, which also augmented with the presence of 50 nM h-iAβo (Fig. 1d, arrows in middle trace). The increase in activity was a concentration-dependent phenomenon, given that there were more bursts of synaptic activity and events of greater amplitude as the concentration of iAβo augmented from 50 to 1000 nM. We integrated the area under the current trace for each condition and computed the charge transferred for the recorded cell (see calculation details in Additional file 1: Supplementary methods, section 1.9). 1000 nM h-iAβo increased significantly the charge transferred meaning that more current by unit of time was flowing through the membrane compared to control conditions (Fig. 1e). Interestingly, 50 and 1000 nM produced an increase in the frequency of the recorded events (Fig. 1f), but only 1000 nM augmented the amplitude (Fig. 1g). To confirm the time course of these results and to validate the method as an approximation to effectively deliver Aβo to the intraneuronal compartment, we repeated this experiment using a fluorescently labeled synthetic Aβo. The results show that Aβo in the patch pipette is rapidly delivered to the

intraneuronal compartment, since the increase in synaptic activity was correlated with a temporal increase in fluorescence, with a $t_{1/2}$ of 29 s (Additional file 1: Supplementary Figure 1).

Concentration-dependent increase of miniature currents by iAβo

It is accepted that in order to record synaptic currents at the postsynaptic site, a release of neurotransmitters must occur from the pre-synaptic terminal (Fig. 1c). To quantify the effect of iAβo on actual synaptic transmission, we recorded miniature post-synaptic currents (mPSCs). Intracellular application of 500 nM of h-iAβo was able to produce a rapid and significant increase in the frequency and amplitude of mPSCs (Fig. 2a - c). This result was confirmed using different concentrations of synthetic iAβo, that compared with control condition, exhibited a significant increase in the number of events as the concentrations was raised, indicating a concentration-dependent effect (Fig. 2d). The effects of iAβo were more evident on the frequency of miniature events since statistically significant differences were already found at 0.5 nM of iAβo when compared to control conditions (Fig. 2e). On the other hand, the effect of iAβo on the amplitude was only significant at a much higher concentration (Fig. 2f, 1000 nM). We wanted to perform some additional experimental controls to evaluate potential confounds with the application of intracellular iAβo. Therefore, we applied reverse sequence Aβo, as well as the vehicle used to dissolve the peptide. Under these conditions, no significant differences in frequency with respect to the control condition were found (Additional file 1: Supplementary Figure 2). Furthermore, we wanted to control whether the osmolarity of the internal solution was affected by adding different iAβo concentrations, but no significant changes were found (Additional file 1: Supplementary Figure 2). Finally, we applied iAβo in the absence and presence of a specific antibody (A11) that recognizes oligomeric forms [26] and found that it significantly attenuated its toxicity (Additional file 1: Supplementary Figure 3).

Human-iAβo affects excitatory/inhibitory (E/I) balance *in vitro*

A great body of evidence indicates that Aβ disrupts excitatory neurotransmission in different AD mice models [27–30] thereby affecting E/I balance [31]. Since our previous results

showed an increase in iAβo-mediated neurotransmission and augmented spike number in current recording mode, we examined whether h-iAβo could specifically affect glutamatergic vs GABAergic neurotransmission and thereby changing the E/I balance in hippocampal neurons. For this, we performed voltage-clamp experiments using a low Cl^- internal solution (see details in section 2.4.1). This allowed us to record EPSC and IPSC separately by changing the membrane holding potential. The results showed that h-iAβo markedly increased the spontaneous excitatory post-synaptic currents (sEPSC) (Fig. 3a, bottom, right trace), but not the inhibitory post-synaptic currents (sIPSC). The data also shows that charge transferred for sEPSC, but not sIPSC, was significantly increased by h-iAβo (Fig. 3b, black bar). Consequently, the E/I balance obtained analyzing charge transferred was highly and rapidly increased by h-iAβo (Fig. 3b, white bar). Since sEPSC are mainly mediated by AMPA receptors in the current experimental conditions, our results suggest that the alteration in AMPA-mediated neurotransmission underlies this excitatory input disruption.

Differential effects of iAβo on isolated excitatory AMPA and inhibitory $GABA_A$ currents.

Subsequently, we studied pharmacologically isolated AMPAergic and GABAergic miniature synaptic currents (2 of the predominant neurotransmissions present in hippocampal neurons [32]) to confirm the selectivity of iAβo. In the presence of iAβo, there was a significant increase in the frequency of AMPA mEPSCs and GABAergic mIPSCs (Fig. 4a and c). On the other hand, only the amplitude of AMPA was affected by iAβo, as clearly seen by the average synaptic event (Fig. 4b). The quantification of these parameters (frequency and amplitude) were plotted to assess the iAβo effects on both types of neurotransmission (Fig. 4e and f). We also performed voltage-clamp recordings in the stratum pyramidale of the CA1 area (SP-CA1) in hippocampal slices of an adult mouse (*ex vivo*) and found similar results (Additional file 1: Supplementary Figure 4). Because the AMPAergic mediated-neurotransmission was more significantly affected, we examined AMPAergic currents in presence of h-iAβo and confirmed that human-derived oligomers also produced the increase in excitatory synaptic transmission (Additional file 1: Supplementary Figure 5). The experimental observation that the amplitude was affected for AMPA receptors (with human-derived and synthetic preparations) was also confirmed by evaluating ligand-evoked

currents in hippocampal neurons. The results showed that the presence of iAβo enhanced the AMPA-mediated current amplitude by about 2 times (Control I normalized: 1.00 ± 0.05 vs. iAβo: 1.95 ± 0.23) (Fig. 4g and i). Once again, this was a specific effect for the excitatory transmission since no effects were observed for GABA-evoked currents (Fig. 4h and i).

The effect of iAβo on AMPA neurotransmission depends on PKC

These previous results prompted us to investigate in depth the mechanism(s) that could be mediating the effect of iAβo on the AMPAergic excitatory transmission. It has been shown that phosphorylation of ionotropic channels plays a preponderant role in the regulation of synaptic function [33], and the intracellular perfusion of an atypical isoform of PKC denominated PKCM (a constitutively active form of PKC) increases the synaptic response mediated by the AMPA receptor in a similar way to what we previously observed in our recordings with iAβo [34]. Taking into account the above, and considering that it is quite a rapid effect, we decided to record AMPA-R currents (miniature and ligand-evoked) in the presence of a PKC inhibitor (CLR, 2.5 µM intracellularly). We found that the effect of iAβo on the frequency and amplitude of the mEPSCs was diminished when co-applied together with CLR (Fig. 5a), as evidenced by quantifying both parameters for all experimental conditions tested with and without inhibitor application (Fig. 5b and c), clearly showing that the effect of iAβo on AMPA mEPSCs was dependent on this kinase. On the other hand, AMPA evoked-currents also showed that iAβo increased the current evoked by AMPA (Fig. 5d) in relation to control, but in the presence of the PKC-inhibitor a significant decrease occurred, reaching values similar to those of control where only CLR was applied (Fig. 5d). Quantification of the amplitude of the evoked EPSC showed a statistically significant increase in presence of iAβo with respect to control conditions(Fig. 5e). This was interesting because it not only demonstrated that PKC was involved in the effect of iAβo on the amplitude of mEPSCs and evoked EPSC (a post-synaptic effect), but also on the frequency of mEPSCs (pre-synaptic effect), suggesting that the global effects of iAβo on the excitatory synapse through this kinase compromises the pre- and post-synaptic compartments.

Increased NO-production in iAβo-treated in recorded (RN) and the neighboring (NN) neurons

The data showed that there was a potent effect on the frequency of mPSCs when iAβo was applied to the postsynaptic neuron, suggesting an increase in the release of neurotransmitters at the pre-synaptic terminal [35]. Could it be that iAβo applied to the postsynaptic neuron affects the release of neurotransmitter from the pre-synaptic neuron? If so, could there be a retrograde mechanism involved in the effect? [36]. Because the effect was rapid, we thought that it could be produced by nitric oxide (NO), a retrograde messenger, known to be involved in presynaptic neurotransmitter release [37–39] and produced by nitric oxide synthase (NOS). It is important to consider that low concentrations of iAβo were used for all the recordings obtained in these experiments, which did not affect mPSCs amplitude, but only its frequency. Under these conditions, we decided to use a non-selective nitric oxide synthase inhibitor (L-NAME) together with the following methodological approach: mPSCs and relative NO levels using a fluorescent probe DAQ were simultaneously recorded (details in section 2.6 and in Additional file 1: Supplementary methods, section 1.8). In addition, not only the fluctuation of the relative levels of NO in the recorded cell (denoted as RN) (Fig. 6a) was quantified, but also of neighboring neurons (denoted as NN) (Fig. 6a). Pre-incubation of hippocampal neurons with L-NAME showed no significant differences in the frequency of miniature currents (Fig. 6b-d), but did significantly decrease the NO levels in RN (Fig. 6e) and in NN (Fig. 6g) when compared to control conditions. The statistical comparison was performed at the end of the recording period (20 min.) (Fig. 6e and g, indicated by the gray box) and plotted as a bar graph for RN (Fig. 6f) and NN (Fig 6h). For its part, iAβo had the expected effect and increased the frequency of mPSCs (Fig. 6b-d). Interestingly, the increase in iAβo-mediated miniature synaptic activity occurred at the same time that NO levels increased in the RN (Fig. 6e-f). More importantly, iAβo not only increased the levels of NO in the RN, but also in NN that did not get iAβo (Fig. 6g-h). Pre-incubation of the neuronal culture with L-NAME reduced the effect of iAβo on mPSCs frequency by ≈ 51% (Fig. 6b-d). This decrease in the frequency of mPSCs correlated well with the decrease in the relative NO levels in the RN and NN (Fig. 6e-h, iAβo + L-NAME). Additionally, this NO-dependent effect was confirmed by co-applying iAβo together with a

donor molecule of NO (SNAP 300 µM) causing a synergistic effect between the two, increasing the frequency of mPSCs in the RN (Additional file 1: Supplementary Figure 6), as well as in the relative levels of NO in both the RN and NN (Additional file 1: Supplementary Figure 6). The opposite effect was observed using iAβo in the presence of the NO chelator C-PTIO (Additional file 1: Supplementary Figure 6). On the other hand, no changes in the effects of iAβo in the frequency of mPSCs were found using a specific inhibitor of inducible NO (iNOS) (Additional file 1: Supplementary Figure 7).

iAβo increased the excitability of hippocampal neurons *in vivo* and *in vitro*

The results showed that the excitatory transmission and E/I balance are strongly affected by human and synthetic iAβo. The CA1 area in the hippocampus (a major center of excitatory neurotransmission) is one of the first areas prone to develop early AD neuropathology in humans and mice models [40–44], therefore, we decided to record hippocampal CA1 pyramidal neurons using whole cell current-clamp recordings in an anesthetized *in vivo* rat model to examine neuronal excitability (Fig. 7a). We found that in the presence of iAβo, the neuron begun spiking in response to lower current stimuli (Fig. 7b). Plotting the number of spikes vs. injected current showed a strong shift of the curve to the left (Fig. c), implying that the cell with iAβo was more excitable. Indeed, the constant rheobase for firing was diminished in neurons treated with iAβo (Fig. 7d). On the other hand, the calculated values for input resistance (R_{in}) and kinetic parameters of action potentials (APs) (amplitude, duration and threshold) in both conditions were similar to control conditions (Additional file 1: Supplementary Figure 8). Furthermore, the recording of resting membrane potentials (Vm), without current injection, evidenced a large increase in Vm fluctuations when iAβo was applied to the neuron (Fig. 7e). Vm fluctuations generated an assortment of local potentials that had more depolarized values in iAβo-treated neurons (Control: -68.02 ± 0.001 v/s iAβo: -63.55 ± 0.004; Fig. 7f) nearing it to the AP firing threshold, which was also evidenced as a significant change in Vm standard deviation (SD) (Fig. 7g). iAβo also increased the chance of spontaneous spike firing (Fig. 7h) (control: 0.003 ± 0.003 Hz vs iAβo: 1.068 ± 0.463 Hz). Post recording

361 immunohistochemical analysis confirmed the location of the recorded neurons in the stratum
362 pyramidale of dorsal hippocampus at CA1 (Fig. 7i – j).

363 After confirming the effects on excitability in an *in vivo* model and with the aim of examining
364 the disease relevance and to contribute mechanistically to the results, we examined neuronal
365 excitability hippocampal neurons. For this, current clamp experiments were performed and the
366 effects of human derived (h-iAβo) and synthetic (iAβo) oligomers were evaluated. In agreement
367 with the previous data, we found that a smaller current injection was required to trigger the firing of
368 action potentials (AP) in the presence of h-iAβo (Fig. 8a). Plotting the number of spikes vs. injected
369 current demonstrated that the stimulus-response curve shifted to the left indicating an increase in
370 neuronal excitability in the presence of h-iAβo (Fig. 8b) together with a reduced rheobase (Fig. 8c).
371 Similar results were obtained for synthetic iAβo in the same model (Additional file 1: Supplementary
372 Figure 9), confirming the effect of human and synthetic preparations on neuronal excitability *in vitro.*

373 We then evaluated if the effect of h-iAβo on action potentials (APs) could be the result of
374 augmented transitory depolarizations at the post-synaptic level due to the increase in AMPAergic
375 neurotransmission. In order to examine this, we applied h-iAβo and recorded the membrane
376 potential (Vm) fluctuations of hippocampal neurons without current injection in the presence and
377 absence of an intracellular voltage-dependent sodium channel (Na_v) blocker (5 mM QX-314). When
378 Na_v were blocked, APs were not evident in the recorded neuron. In control conditions, Vm
379 fluctuations generated a population of local synaptic potentials (Fig. 9a) with an average Vm value
380 of -65.3 ± 0.003 mV (Fig. 9b), while in the presence of h-iAβo there was a significant increase in
381 the number and amplitude of these depolarizing events (Fig. 9a), with an average of -60.6 ± 0.012
382 mV (Fig. 9b), similar to what we observed previously in the *in vivo* model. In the presence of iAβo
383 and QX-314 no major differences were observed in Vm fluctuations, except for the lack of AP spikes
384 (Fig. 9a), showing a similar average Vm value to the one observed when h-iAβo was present (-60.8
385 ± 0.017 mV) (Fig. 9b). On the other hand, Vm in the presence of QX-314 had a similar average
386 value to control condition with an average of -65.1 ± 0.014 mV (Fig. 9a-b, in gray). Similar results
387 were obtained in the presence of synthetic iAβo (Additional file 1: Supplementary Figure 10). It is

interesting to note that in all tested conditions the external application of an AMPA receptor antagonist (CNQX) through the perfusion system attenuated all Vm fluctuations (Fig. 9a), indicating that these changes in membrane potential in our experimental condition were synaptic AMPA-driven potentials. This confirms that the AMPAergic-mediated synaptic input is responsible for the iAβo-mediated hyperexcitability observed in our experiments.

In presence of intracellular QX-314, no spikes (APs) were detected (Fig. 9c, 3th and 4th traces; left-to-right direction) confirming blockade of Na+ channels. We also observed the presence of transitory depolarization (Fig. 9c, arrowheads over 3th trace; from left to right) that were not present in presence of QX-314 alone (Fig. 9c, 4th trace; from left to right). This data indicates that iAβo exerts depolarizations of the post-synaptic membrane even in the absence of APs, which are mediated by AMPA receptors, suggesting that this effect did not depend on the generation of APs at the post-synaptic level, but rather an increase in synaptic transmission at pre- and post-synaptic levels.

In order to rule out the possibility that iAβo was directly affecting intrinsic membrane properties and AP firing, we used a model of dorsal root ganglion neurons (DRG) that do not form synapses *in vitro* to record action potentials in the presence and absence of iAβo. The results showed that iAβo did not affect the AP firing nor did the rheobase constant (Additional file 1: Supplementary Figure 11a-d), contrary to the results found in hippocampal neurons. Additionally, and similar to hippocampal neurons, no significant differences were found in the parameters calculated for the APs evoked in this experiment such as amplitude, duration, and threshold (Additional file 1: Supplementary Figure 11e-g).

4. Discussion

Presence of oligomeric species of Aβ in the intraneuronal domain of the membrane was able to increase neurotransmission through mechanisms that involved pre-and post-synaptic actions that resulted in an increased excitability and spreading of neuronal activation. Because the present findings were obtained with human AD-brain derived and synthetic Aβo, they should contribute with disease-relevant data in a new and significant working model. Furthermore, using *in* vitro models allowed us to mechanistically understand the effects on neurotransmission and excitability that could be important in the initial stages of AD and that is likely occurring in an AD-human brain.

Contrary to previously published data using extracellular Aβ or with more chronic application models [45–50], we did not find any synaptic deficits, instead, iAβo increased excitatory and inhibitory neurotransmissions, but with more marked effects on the former. This raises the question of how could iAβo actions progress to synaptic dysfunction in the first place? In this regard, it has been reported that extracellular Aβ increases glutamate neurotransmission [51] which could lead to excitotoxicity [52–54] together with vesicular depletion over extended periods of time [55,56] [57–59]. If we consider these observations with the effects reported in this study, it is tempting to speculate that, over time, iAβo influences synaptic depletion and this is in agreement with results from murine AD models that show that early intracellular accumulation of Aβo leads to synaptic failure and the onset of cognitive deficits (for further details see [60]), once again emphasizing the importance of iAβo during the pre-symptomatic stage of AD.

Pre-synaptic mechanism: Increase in retrograde synaptic signaling by NO

Simultaneous fluorescence and electrophysiology recordings demonstrated that NO is involved in the pre-synaptic effect of iAβo. The data showed that iAβo applied to the postsynaptic site augmented NO levels globally in the neurons together with the frequency of mPSCs, reflecting an enhanced release of neurotransmitters into the synaptic space [35], which is in agreement with studies that have shown that NO increases neurotransmitter release from the excitatory and

inhibitory synapsis [61–63]. Furthermore, PKC is likely involved in this pre-synaptic effect of iAβo since CLR prevented the iAβo-mediated increase in the mEPSCs frequency (Fig. 10a). In agreement with this notion, it was reported that PKC also participates in pre-synaptic mechanisms mediated by the gas neuromodulator NO [64–66], emphasizing the pathway that iAβo might be using to increase neurotransmission.

The support for NO-signaling involvement in iAβo-mediated pathology is multiple. First, we found that iAβo increased this messenger in an ensemble of neurons. Second, during the development of AD, NO synthases (NOS) increase in rodent models and in human brains [67,68]. Moreover, in pre-symptomatic 3xTg mice, it has been observed that this alterations that favor NO-synthesis occur together with synaptic pathology [68]. Thus, we can hypothesize that unregulated release of NO in AD pathology might have negative consequences for neuronal function. Third, at the cellular level a prolonged release of NO could also cause metabolic, oxidative stress, and dysfunction in organelles such as mitochondria and ER, eventually leading to neuronal death [69–73]. Therefore, the results agree with current studies indicating that NO signaling is altered through different mechanisms during the development of AD.

Post-synaptic mechanism for AMPA transmission potentiation

The data indicate that iAβo caused a post-synaptic potentiation through the increase in the AMPA-mediated current. Generally speaking, a change in mEPSC amplitude is a reflection of a change at the post-synaptic level [74]. However, this is not the only case, since this might also be explained by an increased neurotransmitter content in synaptic vesicles, translating into an increase in the amplitude of post-synaptic currents [75]. This was not the case for iAβo because evoked currents with a saturating concentration of AMPA still increased the amplitude of the current, supporting the idea that the effect was postsynaptic in nature. Physiologically relevant, the amplitude of AMPA-evoked and miniature-AMPAergic currents (mEPSCs) increased in the presence of iAβo, an effect that was largely attenuated in the presence of a PKC inhibitor (CLR). In general, several kinases found in hippocampal neurons, including PKA (Protein kinase A) and

CAMKII (Ca^{2+}/Calmodulin Protein kinase II), can have similar effects may affect AMPA receptors. For example, CAMKII increases AMPA receptor conductance [76] and the number of synaptic physical contacts, improving the connectivity that mediates excitatory transmission [77]. On the other hand, PKA can increase the number of AMPAR at the synapse [78], as well as increase the release of neurotransmitters at the pre-synaptic site [79].

In this regard, Whitcomb and co-workers reported a PKA dependent increase on AMPA current amplitude in response to iAβo in hippocampal slices [80]. However, their results differed from the present because they required longer times of exposure and it was dependent on calcium. The discrepancies may be due to differences in oligomers preparation, time exposure course, or the effective concentration, since in the present study the amplitude increased only with higher concentrations. Interestingly, another study in cultured autaptic hippocampal neurons found that intracellular Aβ decreased neurotransmission by an unknown mechanism [81]. The present results allows us to conclude that the increase in AMPA receptor function represents a main mechanism by which iAβo depolarizes the post-synaptic membrane and increases the probability for action potential firing (Fig. 10c and d).

Implications of pre- and post-synaptic effects at circuit level in AD pathology: NO functional spreading and neural excitability in AD

The question that became evident after finding that iAβo was able to produce large increases in the E/I balance was if this could have a more global consequence on neuronal hyperexcitability. First, we were able to demonstrate that iAβo induced rapid and large modifications of the bioelectric activity of hippocampal neurons leading to an “epileptiform like phenomena”, which was evidenced by the presence of complex discharge activity composed of synaptic depolarization and spike firing, both initiated by an increase in AMPA neurotransmission.

A quite novel result found during our study was that not only the hippocampal neuron that had iAβo became overactive, but also neighboring neurons displayed increases in NO-production in a synchronized fashion. This suggests that there is a phenomenon in which the functional effect

of iAβo extends to surrounding neurons in a coordinated way. In other words, by mechanisms only now beginning to be appreciated, iAβo alters the function of hippocampal neurons beyond where it is physically present, thus, iAβo has an impact at the circuit level (Fig. 10e).

This phenomenon of increased synchronization, closely resembles the effect of prions of the nervous system, which have been shown to spread the pathology through the brain [82,83]. The difference is that in our case there would be no transmission of iAβo *per se*, but only of the functional effects that it produces. Therefore, we have adopted the term "functional spreading" to refer to this phenomenon.

Now, the consequence of increasing NO is functional because as NO is released the probability of increasing the discharge of excitatory neurotransmitters in nearby areas is also increased [84–86], thus increasing neuronal activity, frequency of action potential firing, and excitability of the neural network [71], [87,88]. Also, in an epilepsy model induced by the intrahippocampal injection of kainate, a well-known AMPA receptor agonist, an increase in NOS activity was observed suggesting a direct link between NO and AMPA-mediated epileptiform activity [89]. There is a strong link between AMPAR and epilepsy [90], and the antagonists significantly reduced or nullified epileptiform activity in hippocampal neurons [91,92]. Thus, our results support the existence of a strong relationship between NO and glutamatergic neurotransmission in the genesis of epileptic hyperexcitability, which could be contributing to the neuronal excitability observed in our models and to the epileptiform activity exhibited by murine AD models and more importantly AD patients [14,15,25,93].

Considering our results, it is possible to hypothesize that only a few neurons that with iAβo could initiate the increase in neurotransmission and excitability in the network, initiating an epileptogenic focus and triggering a functional spreading phenomenon for the whole neuronal ensemble, with very disrupting consequences to the brain.

Taken together, our study suggests that iAβo exerts two effects (pre- and post-synaptic) that seem to be site independent for its expression, but both initially triggered signal transduction

pathways (Fig.11 a). They could provide a potential mechanism to explain early stages of AD, when iAβo accumulates, increasing neuronal hyperexcitability and becoming an epileptogenic focus at the AD onset. Therefore, the prevention of early effects of iAβo, which are mainly intracellular, can potentially be a new therapeutic target for AD. Early treatment could partially or totally reverse the molecular mechanisms by which the peptide initially triggers the synaptic impairment observed in patients in more advanced stages of this disease.

5. Conclusions

Taking together *in vitro*, *ex vivo* and *in vivo* data, we conclude that human and synthetic iAβo induce hyperexcitability through a synaptic-driven mechanism involving AMPA receptors and NO as a retrograde signaling molecule. Additionally, we describe a novel phenomenon in which the functional effect of iAβo on NO production extends to surrounding neurons in a coordinated way. These important findings give new a new meaning to intracellular Aβ accumulation, an early event in the pathology, and uncovers a novel mechanistic explanation for the functional spreading of iAβo-mediated hyperexcitability in a neuronal ensemble.

6. Abbreviations

AMPA	α-amino-3-hydroxy-5-methyl-4-isoxazolepropionic acid
APs	Action potentials
APP	Amyloid precursor protein
Aβ	Amyloid-β peptide
CLR	Chelerythrine
EA	Alzheimer's disease
eEPSCs	Evoked excitatory post-synaptic currents
eIPSCs	Evoked inhibitory post-synaptic currents
eNOS	Endothelial nitric oxide synthase
h-iAβo	human AD brain-derived Aβ oligomers
iAβo	synthetic intracellular Aβ oligomers
iNOS	Inducible nitric oxide synthase
mEPSCs	Miniature excitatory post-synaptic currents
mIPSCs	Miniature inhibitory post-synaptic currents
mPSCs	Miniature post-synaptic currents
Na_v	Voltage-dependent sodium channel
nNOS	Neuronal nitric oxide synthase

582 **NO** Nitric oxide

583 **NOS** Nitric oxide synthase

584 **PKC** Protein kinase C

585 **PLC** Phospholipase C

586 **PSEN1** Presenilin-1

587 **TTX** Tetrodotoxin

588 **Vm** Membrane potential

589

590

591

592

593

594

595

596

597

598

599

600

601

602

603

604

605

7. Declarations

Ethics approval

All experimental procedures were according to Institutional Animal Care and Use Committee at the University of Concepción animal research regulations.

Consent for publication

Not applicable

Availability of data and materials

The datasets used and/or analyzed during the current study are available from the corresponding author on reasonable request.

Competing interests

The authors declare that they have no competing interests

Funding

This work was supported by Fondecyt Grants 1140473 (LGA) and 1180752 (LGA). EJFP was supported by PhD Conicyt fellowship 81150045.

Author Contributions

EJFP and LGA designed experiments, discussed the results, contributed to all stages of manuscript preparation and editing. Material preparation, data collection and analysis were performed by EJFP, BM, DAB, CP, NORL, MPE, JPM, CF, RB, US. All authors read and approved the final manuscript.

Acknowledgments

The authors would like to thank Marco Fuenzalida, Juan Pablo Henriquez and Marcela Torrejón for their invaluable comments and for helpful discussion. The authors also thanks Agenor Limon and

628 Lauren Aguayo for having read and provided useful suggestions to the manuscript. For technical
629 support we thank: Laurie Aguayo, César Lara, Daniela Nova, Alejandra Ramírez, Ixia Cid, Javiera
630 Gavilan and Jocelin González.

631

632

633

634

635

636

637

638

639

640

641

642

643

644

645

646

647

648

8. References

1. Selkoe DJ, Hardy J. The amyloid hypothesis of Alzheimer's disease at 25 years. EMBO Mol Med. 2016;

2. Edwards FA. A Unifying Hypothesis for Alzheimer's Disease: From Plaques to Neurodegeneration. Trends Neurosci. 2019.

3. Welikovitch LA, Do Carmo S, Maglóczky Z, Szocsics P, Lőke J, Freund T, et al. Evidence of intraneuronal Aβ accumulation preceding tau pathology in the entorhinal cortex. Acta Neuropathol [Internet]. Springer Berlin Heidelberg; 2018 [cited 2019 Feb 19];136:901–17. Available from: http://link.springer.com/10.1007/s00401-018-1922-z

4. Pensalfini A, Albay 3rd R, Rasool S, Wu JW, Hatami A, Arai H, et al. Intracellular amyloid and the neuronal origin of Alzheimer neuritic plaques. Neurobiol Dis [Internet]. 2014/08/06. 2014;71:53–61. Available from: http://www.ncbi.nlm.nih.gov/pubmed/25092575

5. Oddo S, Caccamo A, Shepherd JD, Murphy MP, Golde TE, Kayed R, et al. Triple-transgenic model of Alzheimer's Disease with plaques and tangles: Intracellular Aβ and synaptic dysfunction. Neuron. 2003;

6. Billings LM, Oddo S, Green KN, McGaugh JL, LaFerla FM. Intraneuronal Abeta causes the onset of early Alzheimer's disease-related cognitive deficits in transgenic mice. Neuron [Internet]. 2005/03/08. 2005;45:675–88. Available from: http://www.ncbi.nlm.nih.gov/pubmed/15748844

7. Oddo S, Caccamo A, Smith IF, Green KN, LaFerla FM. A dynamic relationship between intracellular and extracellular pools of Abeta. Am J Pathol [Internet]. 2006/01/10. 2006;168:184–94. Available from: http://www.ncbi.nlm.nih.gov/pubmed/16400022

8. Wirths O, Bayer TA. Neuron loss in transgenic mouse models of Alzheimer's disease. Int J Alzheimers Dis [Internet]. Hindawi Limited; 2010 [cited 2019 Feb 18];2010. Available from: http://www.ncbi.nlm.nih.gov/pubmed/20871861

673 9. Iulita MF, Allard S, Richter L, Munter LM, Ducatenzeiler A, Weise C, et al. Intracellular Aβ
674 pathology and early cognitive impairments in a transgenic rat overexpressing human amyloid
675 precursor protein: A multidimensional study. Acta Neuropathol Commun. 2014;

676 10. Tomiyama T, Matsuyama S, Iso H, Umeda T, Takuma H, Ohnishi K, et al. A Mouse Model of
677 Amyloid β Oligomers: Their Contribution to Synaptic Alteration, Abnormal Tau Phosphorylation,
678 Glial Activation, and Neuronal Loss In Vivo J Neurosci [Internet].
679 2010;30:4845 LP – 4856. Available from: http://www.jneurosci.org/content/30/14/4845.abstract

680 11. Huijbers W, Mormino EC, Schultz AP, Wigman S, Ward AM, Larvie M, et al. Amyloid-β
681 deposition in mild cognitive impairment is associated with increased hippocampal activity, atrophy
682 and clinical progression. Brain. 2015;

683 12. Dickerson BC, Salat DH, Greve DN, Chua EF, Rand-Giovannetti E, Rentz DM, et al. Increased
684 hippocampal activation in mild cognitive impairment compared to normal aging and AD. Neurology.
685 2005;

686 13. Born HA. Seizures in Alzheimer's disease. Neuroscience. 2015.

687 14. Hommet C, Mondon K, Camus V, De Toffol B, Constans T. Epilepsy and dementia in the elderly.
688 Dement Geriatr Cogn Disord [Internet]. 2008/03/04. 2008;25:293–300. Available from:
689 http://www.ncbi.nlm.nih.gov/pubmed/18311076

690 15. Amatniek JC, Hauser WA, DelCastillo-Castaneda C, Jacobs DM, Marder K, Bell K, et al.
691 Incidence and predictors of seizures in patients with Alzheimer's disease. Epilepsia [Internet].
692 2006/05/12. 2006;47:867–72. Available from: http://www.ncbi.nlm.nih.gov/pubmed/16686651

693 16. Lozsadi DA, Larner AJ. Prevalence and causes of seizures at the time of diagnosis of probable
694 Alzheimer's disease. Dement Geriatr Cogn Disord. 2006;

695 17. Mendez MF, Lim GTH. Seizures in elderly patients with dementia: Epidemiology and
696 management. Drugs and Aging. 2003;

18. Cabrejo L, Guyant-Maréchal L, Laquerrière A, Vercelletto M, De La Fournière F, Thomas-Antérion C, et al. Phenotype associated with APP duplication in five families. Brain. 2006;

19. Snider BJ, Norton J, Coats MA, Chakraverty S, Hou CE, Jervis R, et al. Novel presenilin 1 mutation (S170F) causing Alzheimer disease with lewy bodies in the third decade of life. Arch Neurol. 2005;

20. Marcon G, Giaccone G, Cupidi C, Balestrieri M, Beltrami CA, Finato N, et al. Neuropathological and Clinical Phenotype of an Italian Alzheimer Family with M239V Mutation of Presenilin 2 Gene. J Neuropathol Exp Neurol. 2004;

21. Cuevas ME, Haensgen H, Sepulveda FJ, Zegers G, Roa J, Opazo C, et al. Soluble Abeta(1-40) peptide increases excitatory neurotransmission and induces epileptiform activity in hippocampal neurons. J Alzheimers Dis [Internet]. 2011/02/10. 2011;23:673–87. Available from: http://www.ncbi.nlm.nih.gov/pubmed/21304182

22. Born HA, Kim JY, Savjani RR, Das P, Dabaghian YA, Guo Q, et al. Genetic suppression of transgenic APP rescues Hypersynchronous network activity in a mouse model of Alzeimer's disease. J Neurosci [Internet]. 2014/03/14. 2014;34:3826–40. Available from: http://www.ncbi.nlm.nih.gov/pubmed/24623762

23. Brown JT, Chin J, Leiser SC, Pangalos MN, Randall AD. Altered intrinsic neuronal excitability and reduced Na+ currents in a mouse model of Alzheimer's disease. Neurobiol Aging [Internet]. 2011/07/29. 2011;32:2109 e1-14. Available from: http://www.ncbi.nlm.nih.gov/pubmed/21794952

24. Bezzina C, Verret L, Juan C, Remaud J, Halley H, Rampon C, et al. Early onset of hypersynchronous network activity and expression of a marker of chronic seizures in the Tg2576 mouse model of Alzheimer's disease. PLoS One. 2015;

25. Minkeviciene R, Rheims S, Dobszay MB, Zilberter M, Hartikainen J, Fulop L, et al. Amyloid beta-induced neuronal hyperexcitability triggers progressive epilepsy. J Neurosci [Internet]. 2009/03/20. 2009;29:3453–62. Available from: http://www.ncbi.nlm.nih.gov/pubmed/19295151

722 26. Yoshiike Y, Kayed R, Milton SC, Takashima A, Glabe CG. Pore-forming proteins share
723 structural and functional homology with amyloid oligomers. NeuroMolecular Med. 2007;

724 27. Šišková Z, Justus D, Kaneko H, Friedrichs D, Henneberg N, Beutel T, et al. Dendritic structural
725 degeneration is functionally linked to cellular hyperexcitability in a mouse model of alzheimer's
726 disease. Neuron. 2014;

727 28. Bell KFS, Bennett DA, Cuello AC. Paradoxical upregulation of glutamatergic presynaptic
728 boutons during mild cognitive impairment. J Neurosci. 2007;

729 29. Hascup ER, Broderick SO, Russell MK, Fang Y, Bartke A, Boger HA, et al. Diet-induced insulin
730 resistance elevates hippocampal glutamate as well as VGLUT1 and GFAP expression in
731 AβPP/PS1 mice. J Neurochem. 2019;

732 30. Hascup KN, Hascup ER. Altered neurotransmission prior to cognitive decline in AβPP/PS1
733 mice, a model of Alzheimer's disease. J Alzheimer's Dis. 2015;

734 31. Lei M, Xu H, Li Z, Wang Z, O'Malley TT, Zhang D, et al. Soluble Aβ oligomers impair
735 hippocampal LTP by disrupting glutamatergic/GABAergic balance. Neurobiol Dis. 2016;

736 32. Vizi ES, Kiss JP. Neurochemistry and pharmacology of the major hippocampal transmitter
737 systems: Synaptic and nonsynaptic interactions. Hippocampus. 1998;

738 33. Raymond LA, Blackstone CD, Huganir RL. Phosphorylation of amino acid neurotransmitter
739 receptors in synaptic plasticity. Trends Neurosci. 1993.

740 34. Ling DSF, Benardo LS, Sacktor TC. Protein kinase Mζ enhances excitatory synaptic
741 transmission by increasing the number of active postsynaptic AMPA receptors. Hippocampus.
742 2006;

743 35. Malgaroli A, Tsien RW. Glutamate-induced long-term potentiation of the frequency of miniature
744 synaptic currents in cultured hippocampal neurons. Nature. 1992;

745 36. Suvarna Y, Maity N, Shivamurthy MC. Emerging Trends in Retrograde Signaling. Mol.

746 Neurobiol. 2016.

747 37. Hardingham N, Dachtler J, Fox K. The role of nitric oxide in pre-synaptic plasticity and
748 homeostasis. Front Cell Neurosci. 2013;

749 38. Arancio O, Kiebler M, Lee CJ, Lev-Ram V, Tsien RY, Kandel ER, et al. Nitric oxide acts directly
750 in the presynaptic neuron to produce long-term potentiation in cultured hippocampal neurons. Cell
751 [Internet]. 1996;87:1025–35. Available from: http://www.ncbi.nlm.nih.gov/pubmed/8978607

752 39. Hawkins RD, Son H, Arancio O. Nitric oxide as a retrograde messenger during long-term
753 potentiation in hippocampus. Prog Brain Res [Internet]. 1999/02/05. 1998;118:155–72. Available
754 from: http://www.ncbi.nlm.nih.gov/pubmed/9932440

755 40. Gouras GK, Tsai J, Naslund J, Vincent B, Edgar M, Checler F, et al. Intraneuronal Aβ42
756 accumulation in human brain. Am J Pathol. 2000;

757 41. Padurariu M, Ciobica A, Mavroudis I, Fotiou D, Baloyannis S. Hippocampal neuronal loss in the
758 CA1 and CA3 areas of Alzheimer's disease patients. Psychiatr Danub. 2012;

759 42. Braak H, Alafuzoff I, Arzberger T, Kretzschmar H, Tredici K. Staging of Alzheimer disease-
760 associated neurofibrillary pathology using paraffin sections and immunocytochemistry. Acta
761 Neuropathol. 2006;

762 43. Kerchner GA, Hess CP, Hammond-Rosenbluth KE, Xu D, Rabinovici GD, Kelley DAC, et al.
763 Hippocampal CA1 apical neuropil atrophy in mild Alzheimer disease visualized with 7-T MRI.
764 Neurology. 2010;

765 44. LaFerla FM, Green KN, Oddo S. Intracellular amyloid-beta in Alzheimer's disease. Nat Rev
766 Neurosci [Internet]. 2007 [cited 2014 Mar 21];8:499–509. Available from:
767 http://www.ncbi.nlm.nih.gov/pubmed/17551515

768 45. Puzzo D, Piacentini R, Fá M, Gulisano W, Li Puma DD, Staniszewski A, et al. LTP and memory
769 impairment caused by extracellular Aβ and tau oligomers is APP- dependent. Elife. 2017;

770 46. Takamura A, Sato Y, Watabe D, Okamoto Y, Nakata T, Kawarabayashi T, et al. Sortilin is
771 required for toxic action of Aβ oligomers (AβOs): Extracellular AβOs trigger apoptosis, and
772 intraneuronal AβOs impair degradation pathways. Life Sci. 2012;

773 47. Shankar GM, Bloodgood BL, Townsend M, Walsh DM, Selkoe DJ, Sabatini BL. Natural
774 oligomers of the Alzheimer amyloid-β protein induce reversible synapse loss by modulating an
775 NMDA-type glutamate receptor-dependent signaling pathway. J Neurosci. 2007;

776 48. Klyubin I, Betts V, Welzel AT, Blennow K, Zetterberg H, Wallin A, et al. Amyloid beta protein
777 dimer-containing human CSF disrupts synaptic plasticity: prevention by systemic passive
778 immunization. J Neurosci [Internet]. 2008 [cited 2014 Apr 8];28:4231–7. Available from:
779 http://www.pubmedcentral.nih.gov/articlerender.fcgi?artid=2685151&tool=pmcentrez&rendertype
780 =abstract

781 49. Ding Y, Zhao J, Zhang X, Wang S, Viola KL, Chow FE, et al. Amyloid Beta Oligomers Target
782 to Extracellular and Intracellular Neuronal Synaptic Proteins in Alzheimer's Disease. Front Neurol.
783 2019;

784 50. J. Fernandez-Perez E, Peters C, G. Aguayo L. Membrane Damage Induced by Amyloid Beta
785 and a Potential Link with Neuroinflammation. Curr Pharm Des. 2016;

786 51. Parodi J, Sepúlveda FJ, Roa J, Opazo C, Inestrosa NC, Aguayo LG. Beta-amyloid causes
787 depletion of synaptic vesicles leading to neurotransmission failure. J Biol Chem [Internet].
788 2010;285:2506–14. Available from: http://www.ncbi.nlm.nih.gov/pubmed/19915004

789 52. Mehta A, Prabhakar M, Kumar P, Deshmukh R, Sharma PL. Excitotoxicity: Bridge to various
790 triggers in neurodegenerative disorders. Eur. J. Pharmacol. 2013.

791 53. Olloquequi J, Cornejo-Córdova E, Verdaguer E, Soriano FX, Binvignat O, Auladell C, et al.
792 Excitotoxicity in the pathogenesis of neurological and psychiatric disorders: Therapeutic
793 implications. J. Psychopharmacol. 2018.

794 54. Harkany T, Abrahám I, Timmerman W, Laskay G, Tóth B, Sasvári M, et al. Beta-Amyloid

795 Neurotoxicity Is Mediated By a Glutamate-Triggered Excitotoxic Cascade in Rat Nucleus Basalis.
796 Eur J Neurosci [Internet]. 2000;12:2735–45. Available from:
797 http://www.ncbi.nlm.nih.gov/pubmed/10971616

798 55. Marsh J, Alifragis P. Synaptic dysfunction in Alzheimer's disease: The effects of amyloid beta
799 on synaptic vesicle dynamics as a novel target for therapeutic intervention. Neural Regen. Res.
800 2018.

801 56. Crews L, Masliah E. Molecular mechanisms of neurodegeneration in Alzheimer's disease. Hum
802 Mol Genet [Internet]. 2010 [cited 2014 Mar 25];19:R12-20. Available from:
803 http://www.pubmedcentral.nih.gov/articlerender.fcgi?artid=2875049&tool=pmcentrez&rendertype
804 =abstract

805 57. Reeve AK, Krishnan KJ, Duchen MR, Turnbull DM. Mitochondrial dysfunction in
806 neurodegenerative disorders. Mitochondrial Dysfunct. Neurodegener. Disord. 2012.

807 58. Wallace DC, Lott MT, Procaccio V. Mitochondrial Medicine: The Mitochondrial Biology and
808 Genetics of Metabolic and Degenerative Diseases, Cancer, and Aging. Emery Rimoin's Princ Pract
809 Med Genet. 2013.

810 59. Fong S, Teo E, Ng LF, Chen CB, Lakshmanan LN, Tsoi SY, et al. Energy crisis precedes global
811 metabolic failure in a novel Caenorhabditis elegans Alzheimer Disease model. Sci Rep. 2016;

812 60. Bayer TA, Wirths O. Intracellular accumulation of amyloid-Beta - a predictor for synaptic
813 dysfunction and neuron loss in Alzheimer's disease. Front Aging Neurosci [Internet]. 2010/06/17.
814 2010;2:8. Available from: http://www.ncbi.nlm.nih.gov/pubmed/20552046

815 61. Zanelli S, Naylor M, Kapur J. Nitric oxide alters GABAergic synaptic transmission in cultured
816 hippocampal neurons. Brain Res. 2009;

817 62. McNaught KSP, Brown GC. Nitric Oxide Causes Glutamate Release from Brain Synaptosomes.
818 J Neurochem. 2002;

819 63. Prast H, Philippu A. Nitric oxide as modulator of neuronal function. Prog. Neurobiol. 2001.

820 64. Song T, Hatano N, Kambe T, Miyamoto Y, Ihara H, Yamamoto H, et al. Nitric oxide-mediated
821 modulation of calcium/calmodulin-dependent protein kinase II. Biochem J. 2008;

822 65. Ping P, Takano H, Zhang J, Tang XL, Qiu Y, Li RCX, et al. Isoform-selective activation of protein
823 kinase C by nitric oxide in the heart of conscious rabbits: A signaling mechanism for both nitric
824 oxide- induced and ischemia-induced preconditioning. Circ Res. 1999;

825 66. Leppänen T, Tuominen RK, Moilanen E. Protein kinase C and its inhibitors in the regulation of
826 inflammation: Inducible nitric oxide synthase as an example. Basic Clin. Pharmacol. Toxicol. 2014.

827 67. Lüth HJ, Münch G, Arendt T. Aberrant expression of NOS isoforms in Alzheimer's disease is
828 structurally related to nitrotyrosine formation. Brain Res. 2002;

829 68. Shilling D, Muller M, Takano H, Mak D-OD, Abel T, Coulter DA, et al. Suppression of InsP3
830 Receptor-Mediated Ca2+ Signaling Alleviates Mutant Presenilin-Linked Familial Alzheimer's
831 Disease Pathogenesis. J Neurosci. 2014;

832 69. Andersen JK. Oxidative stress in neurodegeneration: Cause or consequence? Nat Rev
833 Neurosci. 2004;

834 70. Sayre LM, Perry G, Smith MA. Oxidative stress and neurotoxicity. Chem. Res. Toxicol. 2008.

835 71. Steinert JR, Chernova T, Forsythe ID. Nitric oxide signaling in brain function, dysfunction, and
836 dementia. Neuroscientist. 2010.

837 72. Moncada S, Higgs EA. Nitric oxide and the vascular endothelium. Handb Exp Pharmacol. 2006;

838 73. Moncada S, Bolaños JP. Nitric oxide, cell bioenergetics and neurodegeneration. J. Neurochem.
839 2006.

840 74. Manabe T, Renner P, Nicoll RA. Postsynaptic contribution to long-term potentiation revealed
841 by the analysis of miniature synaptic currents. Nature. 1992;

842 75. Kullmann DM, Nicoll RA. Long-term potentiation is associated with increases in quantal content
843 and quantal amplitude. Nature. 1992;

844 76. Lee HK, Barbarosie M, Kameyama K, Bear MF, Huganir RL. Regulation of distinct AMPA
845 receptor phosphorylation sites during bidirectional synaptic plasticity. Nature. 2000;

846 77. Pratt KG, Watt AJ, Griffith LC, Nelson SB, Turrigiano GG. Activity-dependent remodeling of
847 presynaptic inputs by postsynaptic expression of activated CaMKII. Neuron. 2003;

848 78. Esteban JA, Shi SH, Wilson C, Nuriya M, Huganir RL, Malinow R. PKA phosphorylation of
849 AMPA receptor subunits controls synaptic trafficking underlying plasticity. Nat Neurosci. 2003;

850 79. Carroll RC, Nicoll RA, Malenka RC. Effects of PKA and PKC on miniature excitatory
851 postsynaptic currents in CA1 pyramidal cells. J Neurophysiol. 1998;

852 80. Whitcomb DJ, Hogg EL, Regan P, Piers T, Narayan P, Whitehead G, et al. Intracellular
853 oligomeric amyloid-beta rapidly regulates GluA1 subunit of AMPA receptor in the hippocampus.
854 Sci Rep. 2015;

855 81. Ripoli C, Cocco S, Li Puma DD, Piacentini R, Mastrodonato A, Scala F, et al. Intracellular
856 accumulation of amyloid-beta (Abeta) protein plays a major role in Abeta-induced alterations of
857 glutamatergic synaptic transmission and plasticity. J Neurosci [Internet]. 2014/09/19.
858 2014;34:12893–903. Available from: http://www.ncbi.nlm.nih.gov/pubmed/25232124

859 82. Fraser PE. Prions and prion-like proteins. J. Biol. Chem. 2014.

860 83. Domert J, Rao SB, Agholme L, Brorsson AC, Marcusson J, Hallbeck M, et al. Spreading of
861 amyloid-β peptides via neuritic cell-to-cell transfer is dependent on insufficient cellular clearance.
862 Neurobiol Dis. 2014;

863 84. Rowley NM, Madsen KK, Schousboe A, Steve White H. Glutamate and GABA synthesis,
864 release, transport and metabolism as targets for seizure control. Neurochem Int. 2012;

865 85. Meldrum BS. The role of glutamate in epilepsy and other CNS disorders. Neurology. 1994;

866 86. Choi DW, Rothman SM. The Role of Glutamate Neurotoxicity in Hypoxic-Ischemic Neuronal
867 Death. Annu Rev Neurosci. 2003;

868 87. Steinert JR, Robinson SW, Tong H, Haustein MD, Kopp-Scheinpflug C, Forsythe ID. Nitric
869 Oxide Is an Activity-Dependent Regulator of Target Neuron Intrinsic Excitability. Neuron. 2011;

870 88. Balez R, Ooi L. Getting to NO Alzheimer's disease: Neuroprotection versus neurotoxicity
871 mediated by nitric oxide. Oxid. Med. Cell. Longev. 2016.

872 89. Yasuda H, Fujii M, Fujisawa H, Ito H, Suzuki M. Changes in Nitric Oxide Synthesis and Epileptic
873 Activity in the Contralateral Hippocampus of Rats Following Intrahippocampal Kainate Injection.
874 Epilepsia. 2008;

875 90. Honoré T, Davies SN, Dreier J, Fletcher EJ, Jacobsen P, Lodge D, et al. Quinoxalinediones:
876 Potent competitive Non-NMDA glutamate receptor antagonists. Science (80-). 1988;

877 91. McBain CJ, Boden P, Hill RG. The kainate/quisqualate receptor antagonist, CNQX, blocks the
878 fast component of spontaneous epileptiform activity in organotypic cultures of rat hippocampus.
879 Neurosci Lett. 1988;

880 92. Neuman RS, Ben-Ari Y, Cherubini E. Antagonism of spontaneous and evoked bursts by 6-
881 cyano-7-nitroquinoxaline-2,3-dione (CNQX) in the CA3 region of the in vitro hippocampus. Brain
882 Res. 1988;

883 93. Davis KE, Fox S, Gigg J. Increased hippocampal excitability in the 3xTgAD mouse model for
884 Alzheimer's disease in vivo. PLoS One [Internet]. 2014/03/14. 2014;9:e91203. Available from:
885 http://www.ncbi.nlm.nih.gov/pubmed/24621690

886 94. Fernández-Pérez EJ, Sepúlveda FJ, Peters C, Bascuñán D, Riffo-Lepe NO, González-
887 Sanmiguel J, et al. Effect of cholesterol on membrane fluidity and association of Aβ oligomers and
888 subsequent neuronal damage: A Double-Edged Sword. Front Aging Neurosci. 2018;

889 95. Fernández-Pérez EJ, Sepúlveda FJ, Peoples R, Aguayo LG. Role of membrane GM1 on early

890 neuronal membrane actions of Aβ during onset of Alzheimer's disease. Biochim Biophys Acta - Mol
891 Basis Dis. 2017;

892 96. Sengupta U, Guerrero-Muñoz MJ, Castillo-Carranza DL, Lasagna-Reeves CA, Gerson JE,
893 Paulucci-Holthauzen AA, et al. Pathological Interface between Oligomeric Alpha-Synuclein and
894 Tau in Synucleinopathies. Biol Psychiatry. 2015;

895 97. Förstera B, Muñoz B, Lobo MK, Chandra R, Lovinger DM, Aguayo LG. Presence of ethanol-
896 sensitive glycine receptors in medium spiny neurons in the mouse nucleus accumbens. J Physiol.
897 2017;

898 98. Morgan PJ, Bourboulou R, Filippi C, Koenig-Gambini J, Epsztein J. Kv1.1 contributes to a rapid
899 homeostatic plasticity of intrinsic excitability in CA1 pyramidal neurons in vivo. Elife. 2019;

900 99. Schuchmann S, Albrecht D, Heinemann U, Von Bohlen und Halbach O. Nitric oxide modulates
901 low-Mg2+-induced epileptiform activity in rat hippocampal-entorhinal cortex slices. Neurobiol Dis.
902 2002;

903 100. R Development Core Team 3.0.1. A Language and Environment for Statistical Computing. R
904 Found Stat Comput. 2013;

905
906
907
908
909
910
911
912
913
914

Figure legends

Figure 1. Intracellular human derived Aβ oligomers (h-iAβo) increased the synaptic transmission and AP spike firing in hippocampal neurons *in vitro*. a, Western blot analysis of AD brain-derived Aβ oligomers with A11 and generic Aβ antibody 6E10. **b,** AFM image of AD brain-derived Aβ oligomer. Scale bar 100 nm. **c,** Schematic representation of the synaptic recordings, showing the pre-synaptic (Pre-S) and post-synaptic (Post-S) compartment, and the use of the patch electrode to dialyze the cell with h-iAβo and to record membrane currents (electrode do not represent actual size). **d,** Representative synaptic currents recordings (holding potential (V_h) = -60 mV). Bursts of synaptic currents (arrowheads) and spikes in current recording mode (arrows) are observed. **e-g,** Quantification of charge transferred (**e**) frequency (**f**) and amplitude (**g**) of post-synaptic currents. Bars represent the average ± SEM for control (n=6), h-iAβo 50 nM (n=7) and h-iAβo 1000 nM (n=8) cells. One-Way Welch's ANOVA with Games-Howell post-hoc test for (**e**): F(2,9.91)=24.04, p=1.57E-4. p-values for post-hoc test: control vs. h-iAβo 50 nM: 5.68E-3 , control vs. h-iAβo 1000 nM: 1.51E-9 and h-iAβo 50 nM vs. h-iAβo 1000 nM: 6.76E-3. One-Way Welch's ANOVA with Games-Howell post-hoc test for (**f**): F(2,10.69)=32.82, p=2.73E-5. p-values for post-hoc test: control vs. h-iAβo 50 nM: 3.29E-2, control vs. h-iAβo 1000 nM: 1.17E-4, h-iAβo 50 nM vs. h-iAβo 1000 nM: 3.80E-4. One-Way Welch's ANOVA with Games-Howell post-hoc test for (**g**): F(2,11.09)=19.25, p=2.47E-4. p-values for post-hoc test: control vs. h-iAβo 1000 nM: 6.94E-04, h-iAβo 50 nM vs. h-iAβo 1000 nM: 4.67E-4. * denotes p <0.05, ** p <0.005, *** p <0.001.

Figure 2. Effects of intracellular Aβ oligomers on the frequency and amplitude of miniature post-synaptic currents. a, Representative mPSCs traces after applying h-iAβo 0.5 μM (V_h = -60 mV). **b, c,** mPSCs frequency (**b**) and amplitude (**c**) quantification for control (n=5 cells) and h-iAβo 500 nM (n=9 cells). **d,** mPSCs traces for control (n=16) and after applying increasing concentrations of synthetic iAβo 0.5 nM (n=14), 5 nM (n=16), 50 nM (n=16), 500 nM (n=14) and 1000 nM (n=16 cells). **e, f,** mPSCs frequency (**e**) and amplitude (**f**) for each of the conditions described in (**d**). Bar charts represent the average ± SEM. Unpaired Student's t-test for (**b**) (t(12)=-5.845, p=7.89E-05) and unpaired Student's t-test with Welch's correction for (**c**) (t(11.93)=-5.123, p=2.56E-04). One-Way Welch's ANOVA with Games-Howell post-hoc test for (**e**): F(5,86)=13.76, p= 7.15E-10. p-

values for post-hoc test: iAβo 0 nM vs. 0.5 nM: 4.57E-2, iAβo 0 nM vs. 5 nM: 2.73E-4, iAβo 0 nM vs. 50 nM: 2.33E-3, iAβo 0 nM vs. 500 nM: 1.17E-4, iAβo 0 nM vs 1000 nM: 3.11E-3. One-Way Welch's ANOVA with Games-Howell post-hoc test for (**f**): F(5,86)=3.73, p=0.004. p-values for post-hoc test: iAβo 0 nM vs. 1000 nM: 2.01E-3. * denotes p <0.05, ** p <0.005 and *** p <0.001.

Figure 3. h-iAβo induces a shift in excitatory/inhibitory (E/I) balance. a, Spontaneous inhibitory (sIPSC) and excitatory (sEPSC) post-synaptic recordings obtained in absence (control) and presence of 1 µM h-iAβo. In this conditions, reverse potential for Cl^- was ≈ -66 mV, allowing us to record sEPSC at a V_h of -60 mV and sIPSC at +10 mV. Segmented lines show the maximum amplitude observed for sEPSC and sIPSC in control condition (Control Imax). **b,** Charge transferred for sEPSC (E) (unpaired Student's t-test: t(11)=-2.75, p=1.86E-2), charge transferred for sIPSC (I) and E/I ratio for each condition (unpaired Student's t-test: t(11)=-2.73, p=1.93E-2), expressed as percentage of control condition. Bar charts represent the average ± SEM for control (n=7) and h-iAβo (n=6) cells. * denotes p <0.05.

Figure 4. iAβo differentially affected AMPA-R and $GABA_A$-R mediated miniature and evoked PSCs. a - d, Pharmacologically isolated AMPA (**a**) and GABA (**c**) mPSCs in control condition and with iAβo 500 nM at V_h = -60 mV, showing the averaged synaptic current for each condition (**b** and **d**)**. e, f,** mEPSC (n=9) and mIPSC (n=8) frequency (**e**) and amplitude quantification (**f**) for control and iAβo-treated cells. **g, h,** AMPA (**g**) and GABA (**h**) evoked currents in the absence (n=9) and presence of iAβo 1 µM (n=9). Segmented lines indicate maximum current reached (I_{MAX}). **i,** Normalized evoked current amplitude (value corresponding to I_{MAX}) for AMPA and GABA receptors. Bar charts represent the average ± SEM. Unpaired Student's t-test with Welch's correction for mEPSC frequency: t(8.29)=-8.07, p=3.31E-5 and unpaired Student's t-test for mIPSC frequency: t(14)=-7.43, p=3.20E-6. Unpaired Student's t-test for mEPSC amplitude: t(16)=-2.62, p=0.018 and mIPSC amplitude: t(14)=-1.86, p=0.086. Unpaired Student's t-test with Welch's correction for (**i**) AMPA-R: t(16)=-3.83, p=1.4E-3 and $GABA_A$-R: t(16)=0.17, p=0.863. * denotes p < 0.05, ** p <0.005 and *** p <0.001.

Figure 5. The effect of iAβo on AMPAergic miniature and evoked EPSCs is PKC dependent. **a,** mEPSCs recordings obtained for control (n=11), iAβo 500 nM (n=11), chelerythrine (CLR) 2.5 µM + iAβo 500 nM (n=12) and CLR 2.5 µM (n=12) (V_h = -60 mV). **b, c,** mEPSC frequency (**b**) and amplitude quantification (**c**) for each of the conditions described in (**a**). **d,** AMPA evoked current in the absence (n=9) and presence of iAβo 1000 nM (n=9), iAβo co-applied together with CLR (n=11) and CLR (n=11) (V_h = -60 mV). Segmented lines indicate maximum current reached (I_{MAX}). **e,** Average amplitude of AMPA evoked current for each condition in (**d**). Bar charts represent the average ± SEM. One-Way Welch's ANOVA with Games-Howell post-hoc test for (**b**): F(3,42)=6.11, p=0.002. p-values for post-hoc test: control vs iAβo: 2.27E-2, iAβo vs. iAβo + CLR: 1.78E-2, iAβo vs. CLR: 2.07E-3. One-Way Welch's ANOVA with Games-Howell post-hoc test for (**c**): F(3,42)=8.54, p=1.52E-4. p-values for post-hoc test: control vs. iAβo: 2.65E-4, iAβo vs. CLR: 1.23E-2, iAβo vs. iAβo + CLR: 9.49E-4. One-Way Welch's ANOVA with Games-Howell post-hoc test for (**e**): F(3,35)=5.88, p=2.31E-3. p-values for post-hoc test: control vs. iAβo: 3.31E-3, iAβo vs. CLR: 1.10E-2, iAβo vs. iAβo + CLR: 1.49E-2. * denotes p < 0.05, ** p <0.005 and *** p <0.001.

Figure 6. Nitric oxide synthase is important the effects of iAβo on the frequency of miniature synaptic currents in the neuronal ensemble. a, Micrograph showing the area of the culture in which mPSCs were obtained from the recorded neuron (RN), as well as the NO-fluorescence for RN and of the neighboring neurons to RN (NN). **b, c,** Representative recordings (**b**) and quantification of mPSCs frequency (**c**) obtained during the course of 20 minutes in absence (control) and presence of iAβo 200 nM, together with the pre-incubation with L-NAME (200 µM for 20-30 min) (V_h = -60 mV). **d,** Quantification of mPSCs frequency at 20 min (obtained from data marked inside gray rectangle from plot in **c**). **e - h,** Relative levels of NO (expressed as normalized fluorescence) obtained throughout the course of the experiment and at 20' for RN (**e** and **f**, respectively) and NN (**g** and **h**, respectively). Line and bar graphs represent the average ± SEM. Control (n=9), L-NAME (n=8), iAβo (n=11) and iAβo + L-NAME (n=10) for RN and control (n=97), L-NAME (n=102), iAβo (n=119) and iAβo + L-NAME (n=102) for NN. One-Way Welch's ANOVA with Games-Howell post-hoc test for (**d**): F(3,34)=60.309, p=1.07E-13. p-values for post hoc test:

Control vs. iAβo: 1.06E-08, L-NAME vs. iAβo + L-NAME: 7.80E-3, iAβo vs. iAβo + L-NAME: 1.40E-08. One-Way Welch's ANOVA with Games-Howell post-hoc test for (**f**): F(3,34)=21.926, p=4.41E-8. p-values for post hoc test: Control vs. iAβo: 2.53E-05, L-NAME vs. iAβo + L-NAME: 3.03E-3, iAβo vs. iAβo + L-NAME: 1.18E-03. One-Way Welch's ANOVA with Games-Howell post-hoc test for (**h**): F(3,416)=40.763, p=4.11E-23. p-values for post hoc test: Control vs. iAβo: 6.44E-20, L-NAME vs. iAβo + L-NAME: 2.16E-3, iAβo vs. iAβo + L-NAME: 8.85E-09. ** denotes p <0.005, *** p <0.001.

Figure 7. iAβo increased the firing of action potentials evoked by current injection in hippocampal neurons *in vivo*. a, Scheme representing the location of the electrode filled with iAβo to record action potentials in the pyramidal cell layer of CA1 (PY) of rat hippocampus (highlighted in green) (brain image obtained from Allen Institute Brain Atlas). **b,** Representative action potential recordings in absence and presence of 500 µM iAβo. **c,** Relationship between the number of evoked action potentials and the injected current intensity for the experimental conditions described in **b** (two-way ANOVA: F(7,103)=7.983, p=1.01E-7). **d,** Quantification of the rheobase constant (unpaired Student's t-test: t(14)=4.188, p=9.11E-4). **e,** Representative recordings obtained without injection of depolarizing current pulses after stabilizing the resting membrane potential (RMP) to -70 mV. **f,** Vm values histogram and average values of Vm ± SEM. **g, h,** Quantification of standard deviation (SD) values for Vm (**g**) (unpaired Student's t-test: t(14)=-3.445, p=3.94E-3) and spontaneous AP firing frequency (**h**) (Mann-Whitney U-test: U=0, z-score=-3.199, p=1.38E-3). **i,** Epifluorescence micrographs of coronal cuts obtained after the electrophysiological recording, showing a positive staining for calbindina-D28k (in green, $\mathbf{i_1}$) and streptavidin (in red, $\mathbf{i_2}$), in hippocampus-CA1. The recorded neuron ($\mathbf{i_3}$) is also observed. DG, dentate gyrus; PY, pyramidal cell layer of CA1; RAD, stratum radiatum. **j,** Confocal micrographs, demonstrating the positive staining for streptavidin in the recorded neuron (in red, $\mathbf{j_2}$) as well as the merge with calbindina-D28k ($\mathbf{j_3}$) within the stratum pyramidale of the CA1 region of the hippocampus. Bar and line charts represent the average ± SEM for control (n=10) and h-iAβo (n=6) cells of at least 6 rats. ** denotes p <0.005, *** p <0.001.

Figure 8. Intracellular human derived Aβ oligomers (h-iAβo) increased the firing of action potentials in hippocampal neurons *in vitro*. a, Hippocampal neuron action potential (AP) recordings in the absence and presence of 500 nM h-iAβo. **b,** Relationship between the number of AP spikes and the injected current intensity for the experimental conditions described previously (two-way ANOVA: F(8,79)=9.077, p=9.31E-9). **c,** Rheobase constant decreased ≈45% for h-iAβo condition (unpaired Student's t-test: t(9)=2.737, p=2.29E-2). Bars and line charts represent the average ± SEM for control (n=6) and h-iAβo (n=5) cells. * denotes p <0.05, *** p <0.001.

Figure 9. Intracellular blockade of voltage-regulated Na_v channels does not prevent depolarization of the membrane activated by h-iAβo. a, Representative recordings obtained without current injection, showing membrane potential (Vm) fluctuations under the different conditions tested. External application of CNQX 20 µM inhibited the fluctuations at great extent in all conditions. **b,** Histogram showing the distribution of Vm values in the different experimental conditions shown in **a**, along with the Vm SD (inset bar graph) One-Way Welch's ANOVA with Games-Howell post-hoc test for: F(3,19)=11.299, p=1.77E-4. p-values for post hoc test: Control vs. iAβo: 7.13E-3 and QX-314 vs. QX-314 + iAβo: 2.12E-3). **c,** Current injection experiments demonstrating that, under the control and h-iAβo conditions, the generation of action potentials was not inhibited, while Na_v intracellular block by QX-314 prevented spiking of neurons with h-iAβo and without it. Arrowheads over 3th trace (left-to-right direction) indicate the presence of depolarizing post-synaptic potentials when h-iAβo was present. This did not occurred for the condition with QX-314 alone (4th trace; left-to-right direction). Bars represent the average ± SEM for control (n=6), h-iAβo (n=5), h-iAβo+QX-314 (n=6) and QX-314 (n=6) cells. * denotes p < 0.05, ** p <0.005 and *** p <0.001.

Figure 10. Scheme depicting the effects of intracellular effects of Aβo on neurotransmission and neuronal excitability. Schematic summary of iAβo actions at the pre- and post-synaptic levels, highlighting a synaptic and a circuit component. At synaptic level, being present in the post-synaptic compartment activates PKC (**a**), which in turn mediates the activation of nitric oxide

synthase (NOS). This triggers the production of nitric oxide (NO) at the post-synaptic level, which, through a retrograde mechanism, activates an increase in the release of neurotransmitters from the pre-synaptic compartment (**b**). These activate the post-synaptic receptors AMPAR (pink) and GABA (in green), which was globally evidenced as an increase in the frequency of GABAergic and AMPAergic mPSCs, respectively. Additionally, PKC present in the post-synapse increases the AMPA receptor current (**c**), increasing post-synaptic depolarization, facilitating the approach of Vm to the threshold and generating action potentials more easily. This directly affects the neuronal function, increasing the excitability of the cell (**d**). Finally, at the circuit level, iAβo in the recorded neuron increased synchronization NO production in nearby neurons that don't have iAβo, a phenomenon we named as "functional spreading" (**e**).

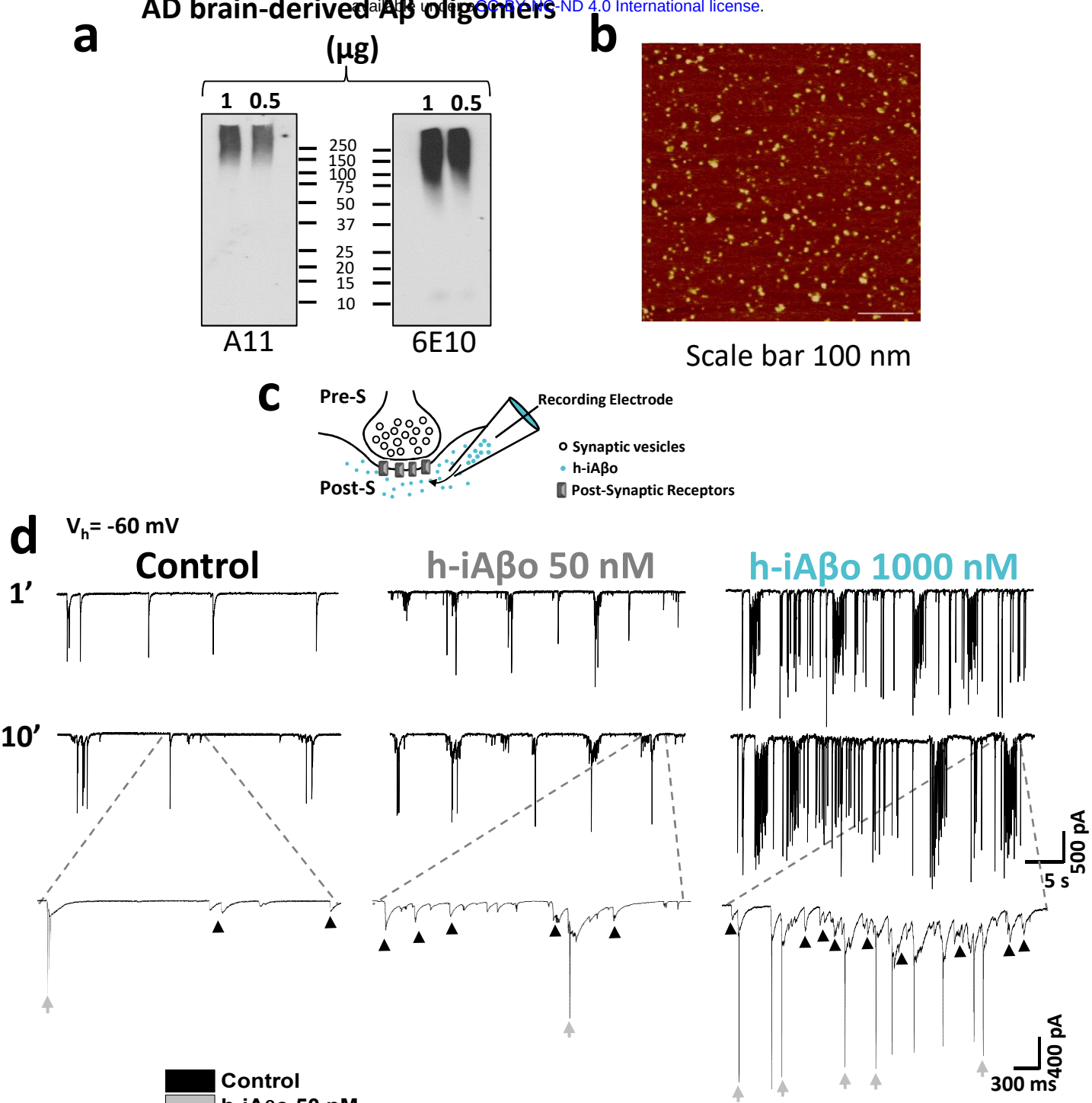

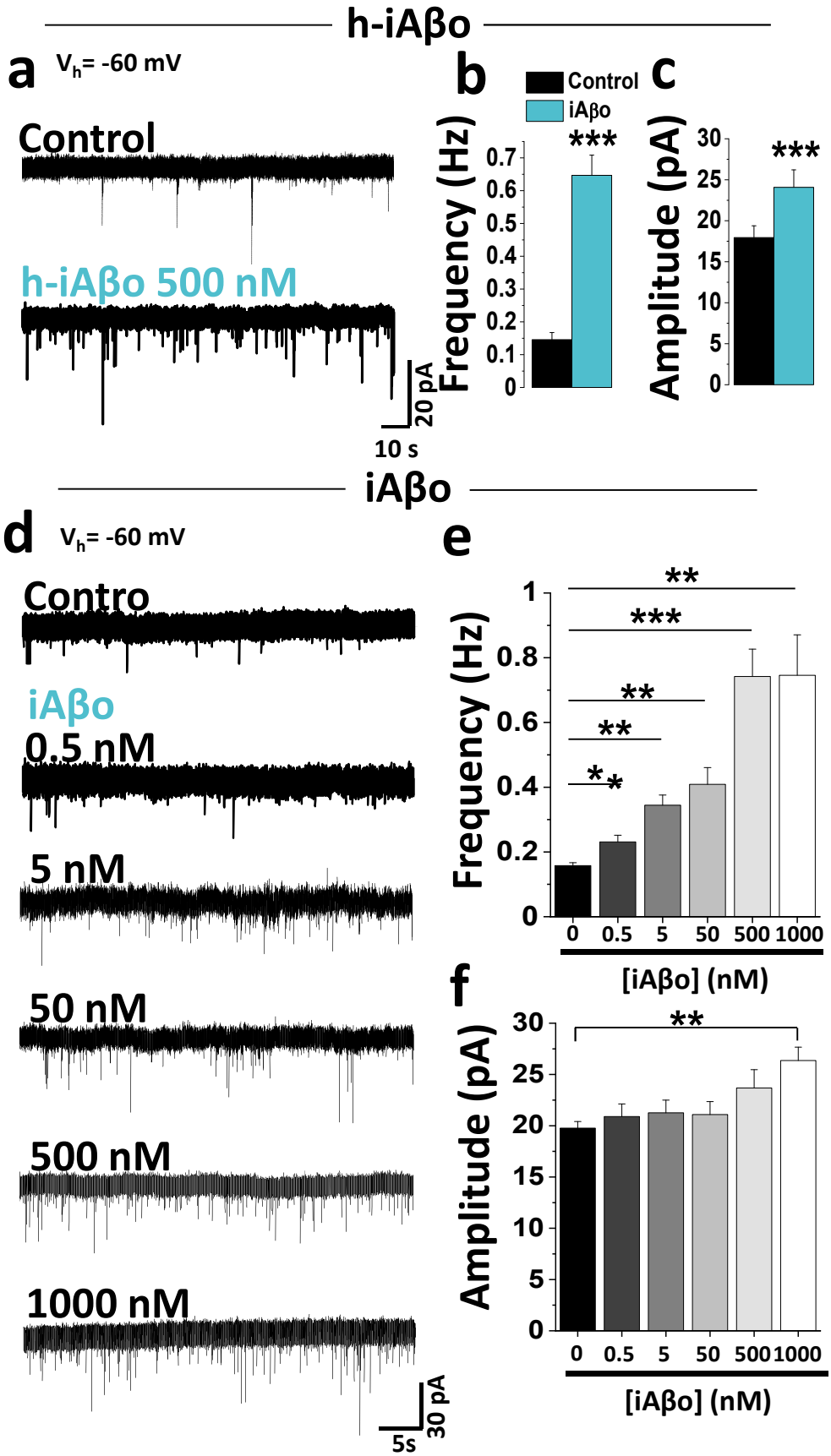

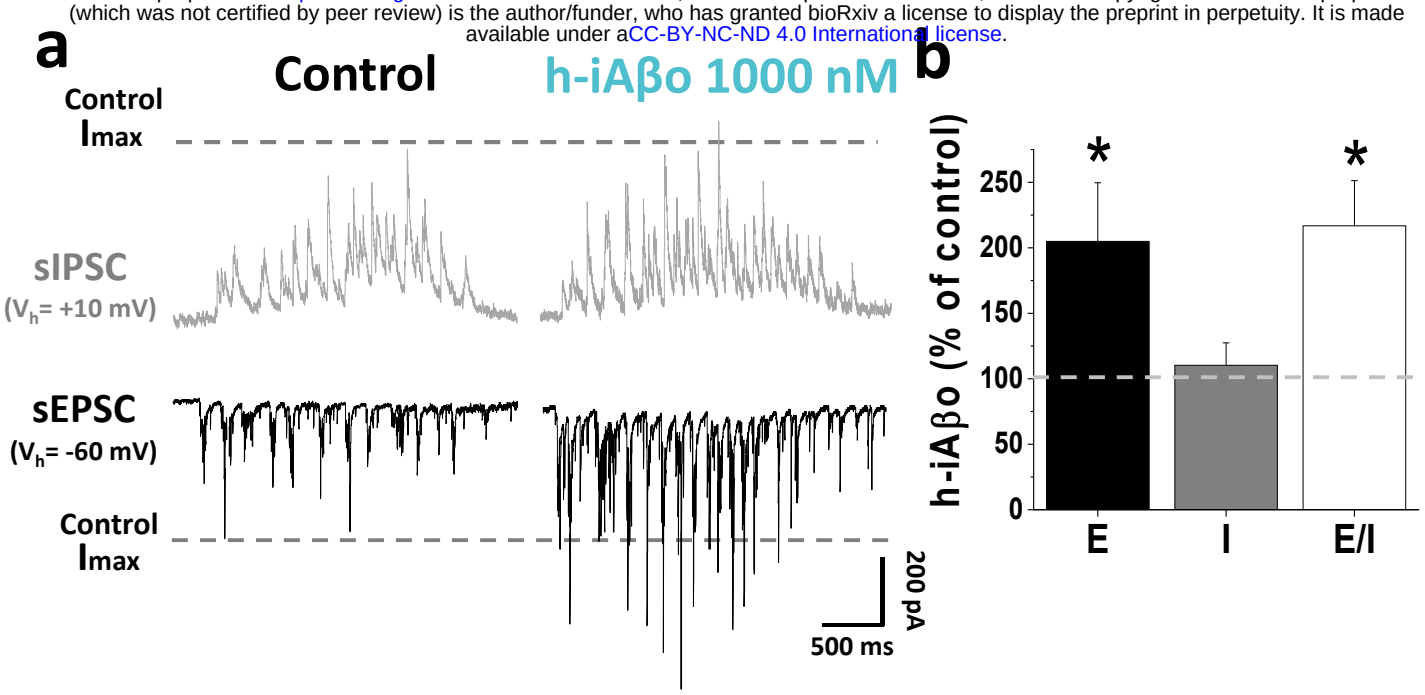

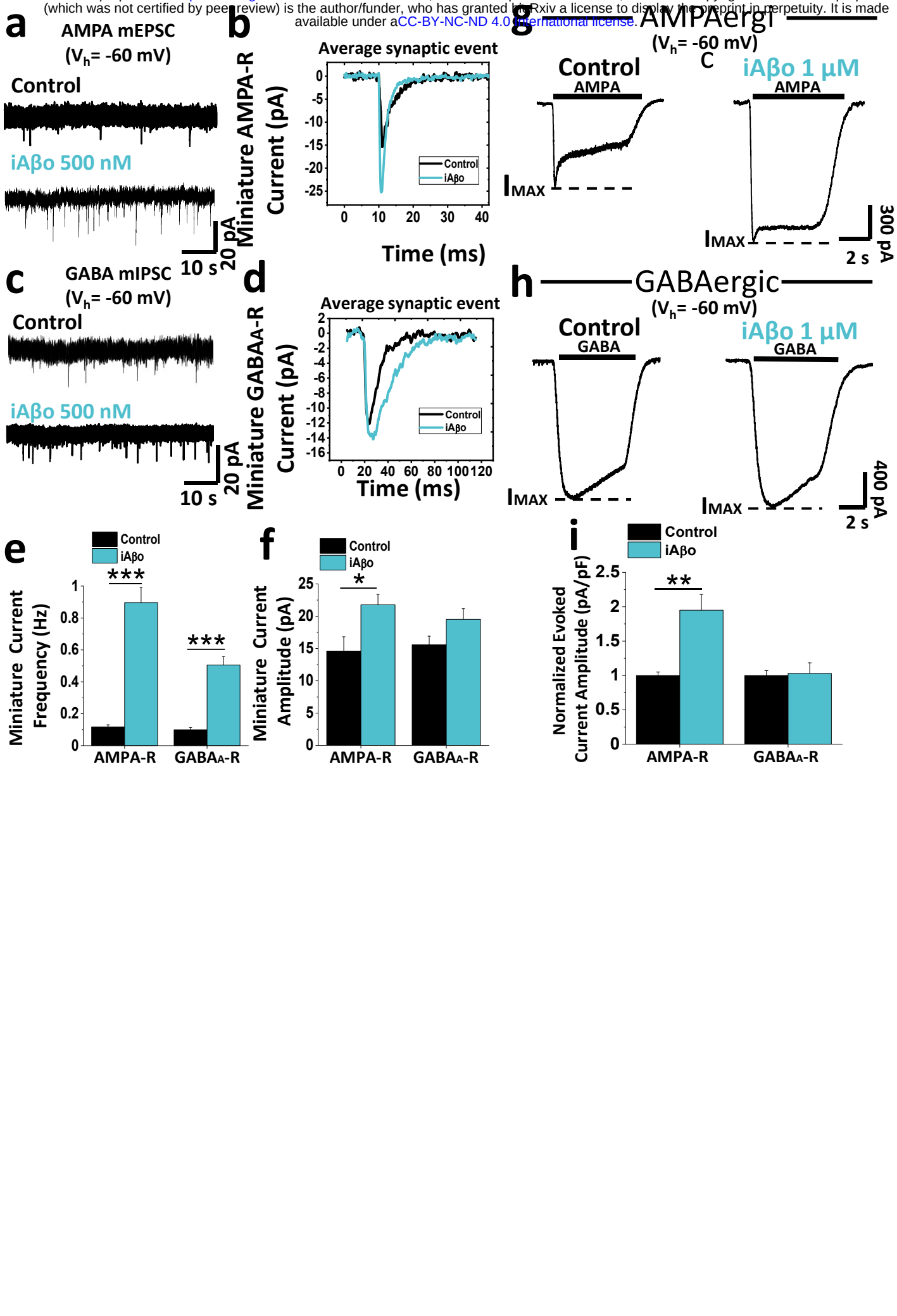

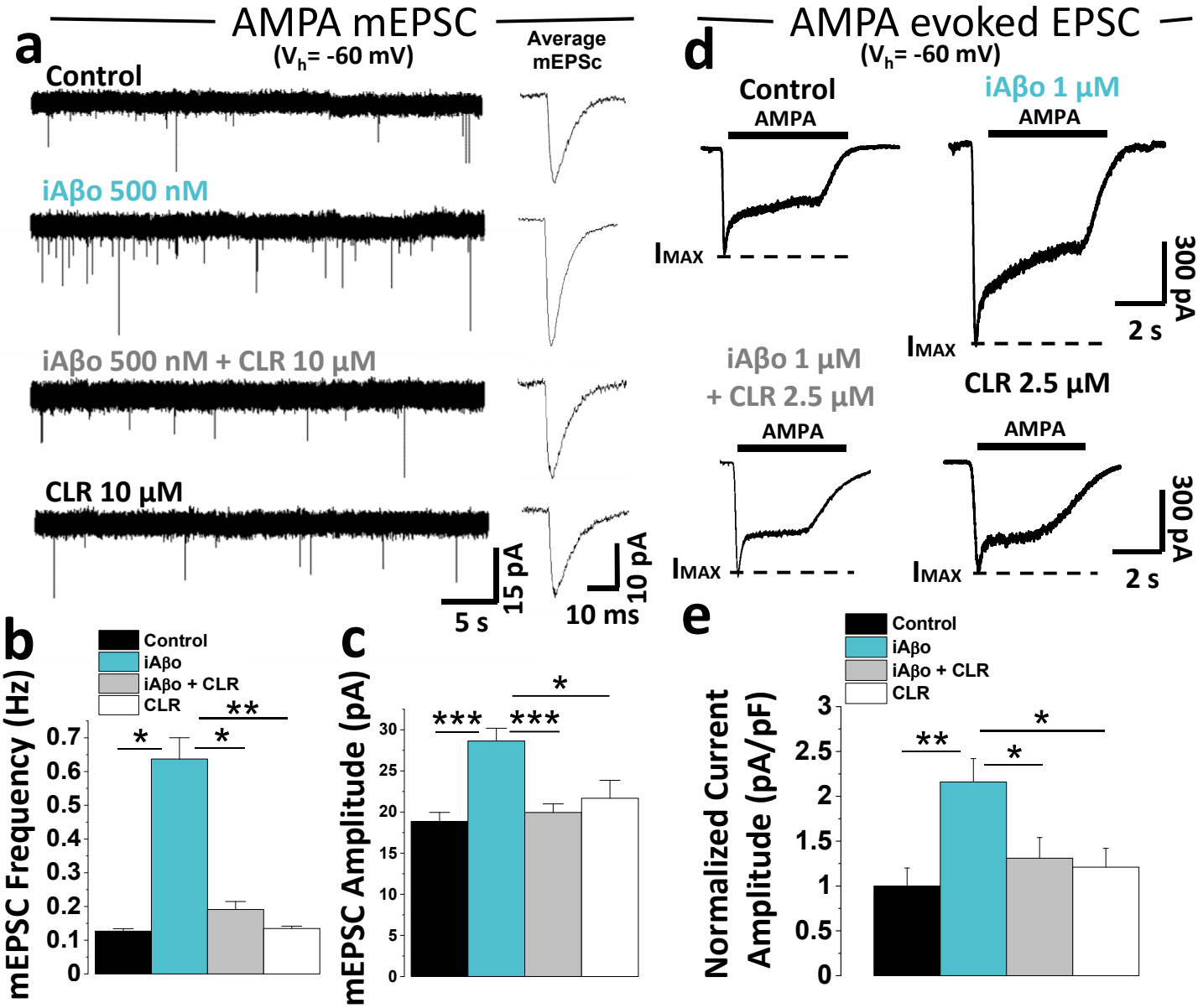

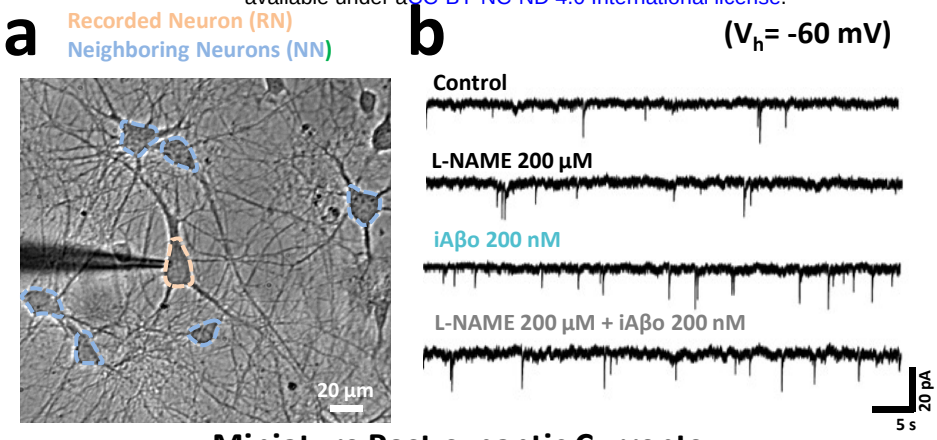

Miniature Post-synaptic Currents

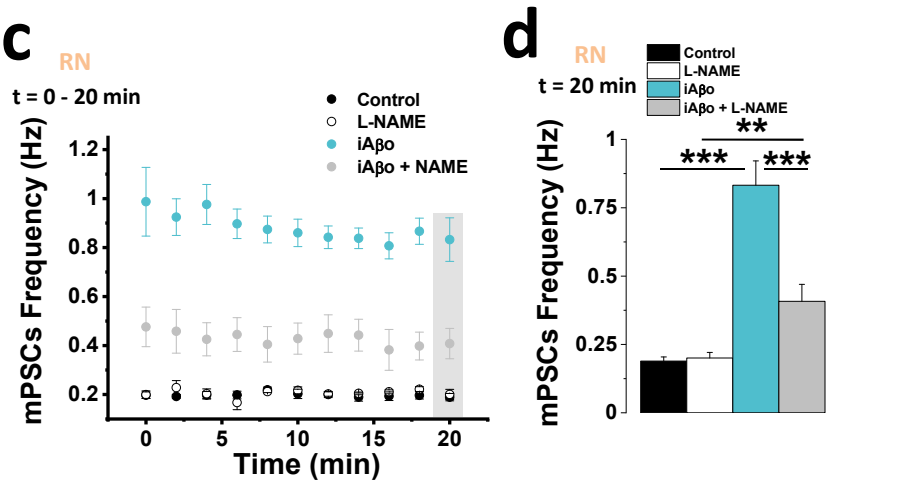

NO fluorescence measurements